

# Self-Assembled Monolayers of A $\beta$ peptides on Au Electrodes: An Artificial Platform for Probing the Reactivity of Redox Active Metals and Cofactors Relevant to Alzheimer's Disease

Debajyoti Pramanik,<sup>†</sup> Kushal Sengupta,<sup>†</sup> Soumya Mukherjee, Somdatta Ghosh Dey,<sup>\*</sup> and Abhishek Dey<sup>\*</sup>

Department of Inorganic Chemistry, Indian Association for the Cultivation of Science, Jadavpur, Kolkata, India, 700032

## S Supporting Information

**ABSTRACT:** The water-soluble hydrophilic part of human A $\beta$  peptide has been extended to include a C-terminal cysteine residue. Utilizing the thiol functionality of this cysteine residue, self-assembled monolayers (SAM) of these peptides are formed on Au electrodes. Atomic force microscopy imaging confirms formation of small A $\beta$  aggregates on the surface of the electrode. These aggregates bind redox active metals like Cu and cofactors like heme, both of which are proposed to generate toxic partially reduced oxygen species (PROS) and play a vital role in Alzheimer's disease. The spectroscopic and electrochemical properties of these Cu and heme bound A $\beta$  SAM are similar to those reported for the soluble Cu and heme bound A $\beta$  peptide. Experiments performed on these A $\beta$ -SAM electrodes clearly demonstrate that (1) heme bound A $\beta$  is kinetically more competent in reducing O<sub>2</sub> than Cu bound A $\beta$ , (2) under physiological conditions the reduced Cu site produces twice as much PROS (measured *in situ*) than the reduced heme site, and (3) chelators like clioquinol remove Cu from these aggregates, while drugs like methylene blue inhibit O<sub>2</sub> reactivity of the heme cofactor. This artificial construct provides a very easy platform for investigating potential drugs affecting aggregation of human A $\beta$  peptides and PROS generation by its complexes with redox active metals and cofactors.



## 1. INTRODUCTION

Alzheimer's disease (AD) is a terminal neurodegenerative disorder with complex etiology. After a slow and silent preclinical phase, memory loss and irreversible brain disorder are the first signs of AD.<sup>1,2</sup> With the progression of the disease other pathological features like confusion, mood swing, and decline of thinking ability become prominent. Current statistics clearly indicate that with the gradual increase of life expectancy, AD has become a serious threat for mankind.<sup>3,4</sup>

The complex nature of this disease is a major obstacle for a curative treatment of AD. The amyloid hypothesis first proposed aggregation of the amyloid  $\beta$  (A $\beta$ ) peptides in different parts of the brain as the key pathological feature of the disease.<sup>5</sup> Extracellular amyloid plaques and intracellular neurofibrillar tangles are two major biomarkers of AD.<sup>6,7</sup> A $\beta$  is a 40–42 amino acid containing peptide which originates from a larger amyloid precursor protein (APP).<sup>8</sup> APP is a trans membrane protein containing 770 amino acids. Proteolysis of APP by  $\beta$ - and  $\gamma$ -secretases produces soluble A $\beta$  peptides in the biological fluid.<sup>9,10</sup> Recent developments in this field suggest small soluble oligomeric forms or pore-like protofibrils of A $\beta$  are more toxic compared to fibrillar forms.<sup>11</sup> Self-aggregation of A $\beta$  is an inadequate postulate to explain the aggregation of A $\beta$  in specific regions of the brain. Thus the role of transition-metal ions in A $\beta$  aggregation has gained focus. Zn, Cu, and Fe dyshomeostasis and their higher concentration in the neocortex of the brain in AD patients reveal the role of these transition metals (Zn<sup>2+</sup>, Cu<sup>2+</sup>, and Fe<sup>3+</sup> to a lesser extent) in the amyloidogenesis of A $\beta$ .<sup>12–14</sup>

Treatment of these A $\beta$  aggregates with metal chelators regenerates soluble A $\beta$ , confirming the role of transition metals in A $\beta$  aggregation.<sup>15,16</sup>

Redox active metals (Fe and Cu) bind to these A $\beta$  peptides and lead to oxidative stress in the brain.<sup>17–19</sup> Under physiological conditions, transition metals and cofactors bound A $\beta$  peptides can spontaneously generate harmful partially reduced oxygen species (PROS, like O<sub>2</sub><sup>-</sup>, O<sub>2</sub><sup>2-</sup>, OH<sup>•</sup>, etc.).<sup>20,21</sup> Highly reactive hydroxyl radicals generate lipid peroxidation adducts and nucleic acid adducts, characteristics of AD pathology.<sup>22–24</sup> PROS formation often oxidize side chains of A $\beta$  peptides to form soluble cross-linked dimers.<sup>25</sup> This process may precede amyloidogenesis, the hallmark physiology of patients diagnosed with AD.<sup>20,25</sup>

Recent studies show that cofactor-like heme (the iron bound protoporphyrin IX cofactor present in hemoglobin and myoglobin) binds to A $\beta$  peptides.<sup>17–19</sup> The heme bound A $\beta$  peptides behave as a peroxidase enzyme.<sup>18,19</sup> These heme–A $\beta$  peptide complexes catalyze the oxidation of neurotransmitters like serotonin and 3,4-dihydroxyphenylalanine (DOPA) by H<sub>2</sub>O<sub>2</sub> and hence could be a possible reason behind the abnormal neurotransmission observed in AD.<sup>19</sup> It has been reported that heme and Cu can bind A $\beta$  simultaneously.<sup>26</sup> In fact, the amount of toxic PROS formation by heme–Cu–A $\beta$  is much higher compared to heme–A $\beta$  or Cu–A $\beta$  complexes. It has also been

Received: April 24, 2012

Published: June 18, 2012

invoked that heme- $A\beta$  complex formation prevents  $A\beta$  aggregation and reduces cytotoxicity.<sup>27</sup>

The complex nature of the pathological features of AD makes it challenging to find out the exact molecular mechanism behind AD and prohibits the possibility of a single therapeutic agent.<sup>28</sup> Some cholesterol lowering drugs (e.g., simvastatin, lovastatin, etc.) have reduced the risk of AD by reducing the intracellular and extracellular levels of  $A\beta(1-40)$  and  $A\beta(1-42)$ .<sup>29,30</sup> Some antioxidants have also slowed down the progression of AD by reducing intraneuronal oligomeric  $A\beta$ .<sup>31,32</sup> Clioquinol is a copper chelating drug that has reduced the risks from redox active Cu center significantly.<sup>33</sup> More recent research suggests mitochondrial dysfunction as the most significant biomarker of AD.<sup>34-36</sup> It has been shown that enhancement of mitochondrial function and maintenance of mitochondrial structural integrity using therapeutics (e.g., methylene blue, MB) reduce the risk of AD.<sup>37</sup>

Human  $A\beta(1-16)$  has been shown to reproduce the metal and cofactor binding properties of  $A\beta(1-40)$  in solution.<sup>18,19,26,38</sup> In this study, human  $A\beta(1-16)$  is appended with a cysteine residue ( $A\beta_{Cys}$ ) at the C-terminus. This cysteine residue bears a thiol group that has been used to form self-assembled monolayers (SAM) on Au electrodes. This heterogeneous surface has been characterized by atomic force microscopy (AFM), absorption spectroscopy, and surface enhanced resonance Raman spectroscopy (SERRS) and has been compared with the solution counterpart. Transition-metal binding property is eminent in this heterogeneous platform. Cyclic voltammetry (CV) and  $O_2$  reducing properties of metal and cofactor bound surfaces of WT and mutant  $A\beta$  provide insight into their reactivity. This artificial platform has been used for probing the effect of potential drugs of AD at low concentrations.

## 2. MATERIALS AND METHODS

All reagents were of the highest grade commercially available and were used without further purification.  $A\beta(1-16)$  peptides appended with a terminal cysteine,  $A\beta_{Cys}$  (sequence: Asp-Ala-Glu-Phe-Arg-His-Asp-Ser-Gly-Tyr-Glu-Val-His-His-Gln-Lys-Cys), Arg<sup>5</sup>Gly, and Tyr<sup>10</sup>Gly mutants of  $A\beta_{Cys}$  have been used for this study. All peptides were purchased from GL Biochem (Shanghai) Ltd. with >95% purity. Hemin, copper sulfate, MB, 8-hydroxy quinoline, octanethiol ( $C_8SH$ ), potassium hexafluorophosphate ( $KPF_6$ ), and the buffers were purchased from Sigma-Aldrich. Disodium hydrogen phosphate dihydrate ( $Na_2HPO_4 \cdot 2H_2O$ ) and imidazole were purchased from Merck. Au wafers were purchased from Platypus Technologies (1000 Å of Au on 50 Å of Ti adhesion layer on top of a Si(III) surface). Transparent Au wafers (100 Å of Au on 10 Å of Ti) were purchased from Phasis, Switzerland. Au and Ag discs for the rotating ring disk electrochemical (RRDE) and SERRS experiments were purchased from Pine Instruments, USA.

**2.1. Instrumentation.** A spectrophotometer (Agilent technologies, model 8453) fitted with a diode-array detector was used to obtain absorption data. All electrochemical experiments were performed using a CH Instruments (model CHI710D Electrochemical Analyzer). Bipotentiostat, reference electrodes, Teflon plate material evaluating cells (ALS Japan) were purchased from CH Instruments. The RRDE set up from Pine Research Instrumentation (E6 series ChangeDisk tips with AFE6M rotor) was used to obtain the RRDE data. The AFM data were obtained at room temperature in a Veeco dcp II (model no.: AP-0100) instrument bearing a phosphate doped Si cantilever (1–10  $\Omega$ -cm, thickness 3.5–4.5  $\mu$ m, length 115–135  $\mu$ m, width 30–40  $\mu$ m, resonance frequency 245–287 kHz, elasticity 20–80 N/m). Solution and surface enhanced resonance Raman spectroscopy data were obtained using a Trivista 555 spectrograph (Princeton Instruments) and using 413.1 nm excitation from a Kr<sup>+</sup> laser (Coherent, Sabre Innova SBRC-DBW-K).

**2.2. Absorption Spectroscopy.** For homogeneous absorption spectroscopy, hemin solution,  $A\beta(1-16)$  peptide solution, and MB

solution were used. Hemin solution was made in 1 N NaOH solution,  $A\beta$  solution was made in 100 mM pH 7 phosphate buffer, and MB solution in triple distilled water. Heme- $A\beta$  solutions were prepared by incubating 1:1 heme: $A\beta$  for ~2 h. For measuring absorption 15  $\mu$ M of the above-mentioned heme- $A\beta$  solution in 100 mM pH 7 phosphate buffer was used. For the heterogeneous absorption experiment, covalently attached heme on modified transparent Au electrodes was used.

**2.3. Electrocatalytic Oxygen Reduction.** **2.3.1. Formation of Mixed SAM.** Gold wafers were cleaned electrochemically, first by electrolysis where it was held at a high positive potential (2.1 V) for few seconds and then by sweeping several times between 1.5 to -0.3 V in 0.5 M  $H_2SO_4$ . SAM solutions contain 0.1 mM  $A\beta(1-17)$  or its corresponding mutants in 100 mM phosphate buffer. Freshly cleaned Au wafers or discs were thoroughly rinsed with triple distilled water and purged with  $N_2$  gas and immersed in the SAM solution for 2 days. After 2 days the substrates were immersed in 0.1 mM  $C_8SH$  (in EtOH) solution for 30 min before electrochemical experiments.

**2.3.2. Attachment of Heme and Copper on to SAM.** Gold wafers or discs immersed in the deposition solution were taken out and rinsed with triple-distilled deionized water in order to remove any excess adsorbate and dried with  $N_2$  gas to remove residual solvent. The wafers were then inserted into a Plate Material Evaluating Cell (ALS Japan) and the discs were mounted on a platinum ring disk assembly (Pine Instruments, USA). As the incubating solutions, 1 mM hemin solution and 10  $\mu$ M  $CuSO_4$  solution in DMSO were used. Heme- $A\beta$  and Cu- $A\beta$  surfaces were prepared by incubating the modified Au surfaces with the respective DMSO solutions for 10 min and 2 h, respectively. For preparing heme-Cu- $A\beta$  surfaces, the modified Au surfaces were incubated with a 1 mM heme +10  $\mu$ M Cu solutions for 2 h. For both Cu- $A\beta$  and heme-Cu- $A\beta$ , the surfaces, after incubation with respective solutions, were rinsed with DMSO for 3 min and then washed with copious amount of deionized water to remove excess physisorbed Cu. Further washing of the electrode with water/DMSO did not lead to Cu loss (Figure S1A, Supporting Information).

**2.3.3. Cyclic Voltammetry Experiments.** All CV experiments were done in pH 7 buffer (until otherwise mentioned) containing 100 mM  $Na_2HPO_4 \cdot 2H_2O$  and 100 mM  $KPF_6$  (supporting electrolyte) using Pt wire as the counter electrode and Ag/AgCl as the reference electrode. Multiple scans with varying scan rates were performed to ensure that Cu was bound to the  $A\beta$  peptide at both reducing and oxidizing potentials (Figure S1B, Supporting Information). Plot of current vs scan rate shows a linear behavior as expected for surface immobilized species (Figure S1B, Supporting Information).<sup>39</sup>

**2.3.4. PROS Experiment.** The platinum ring and the gold disk were both polished by alumina powder (size: 1, 0.3, and 0.05  $\mu$ m) and electrochemically cleaned (as mentioned above for Au wafers) and inserted into the RRDE tip which is then mounted on the rotor and immersed into a cylindrical glass cell, which is equipped with Ag/AgCl reference and Pt counter electrodes. The collection efficiency of the RRDE setup is measured in a 2 mM  $K_3[Fe(CN)_6]$  and 0.1 M  $KNO_3$  solution at 10 mV/s scan rate and 300 rpm rotation speed. The collection efficiency (CE) generally recorded during these experiments was  $20 \pm 2\%$ . The potential at which the ring was held during the collection experiments for detecting  $H_2O_2$  was obtained from literature.<sup>40</sup>

**2.3.5. Inhibition of Catalytic  $O_2$  Reduction of Cofactor- $A\beta$  Complexes.** Inhibition by MB and 8-hydroxy quinoline was studied by using 15  $\mu$ M and 15 nM solutions, respectively, in pH 7 buffer in each case.

**2.4. Solution Resonance Raman and SERRS.** Heme- $A\beta$  solutions of 0.5 mM concentrations were used for obtaining solution resonance Raman spectra at 10 mW power.

For SERRS experiments, Ag discs were cleaned using alumina powder (grit sizes 1, 0.3, and 0.05  $\mu$ m), roughened,<sup>41,42</sup> and immersed in solutions of  $A\beta_{Cys}$  analogous to the Au substrates. The discs were then inserted into the RRDE setup. The experimental set up for collecting SERRS data using a RRDE assembly will be published elsewhere.

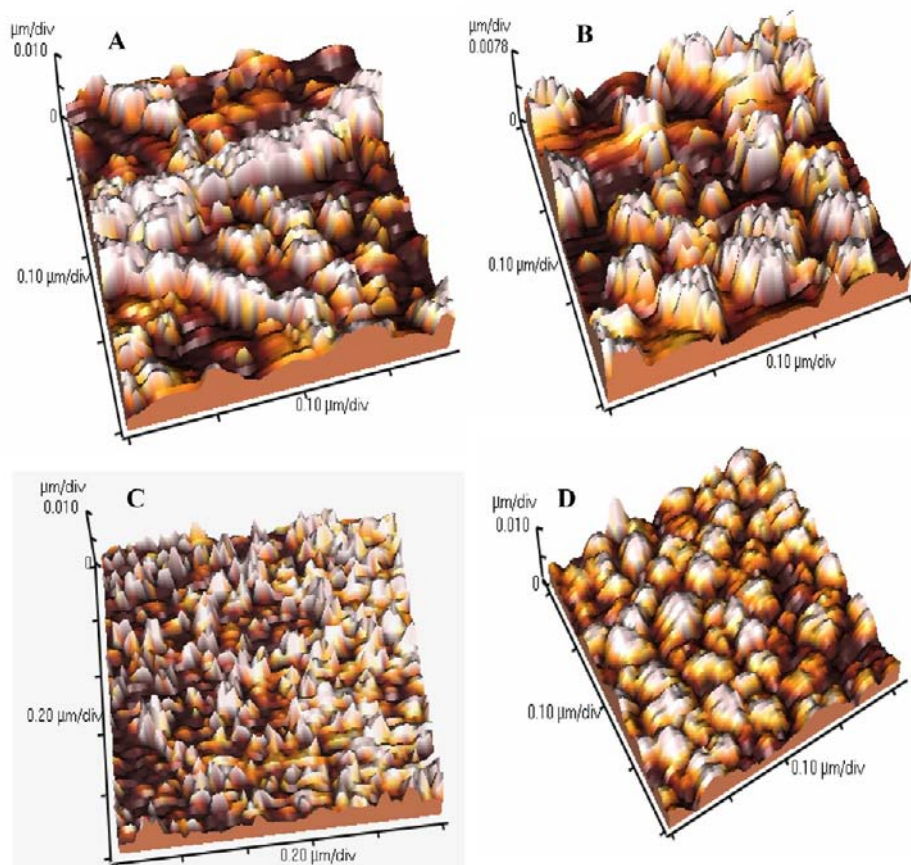
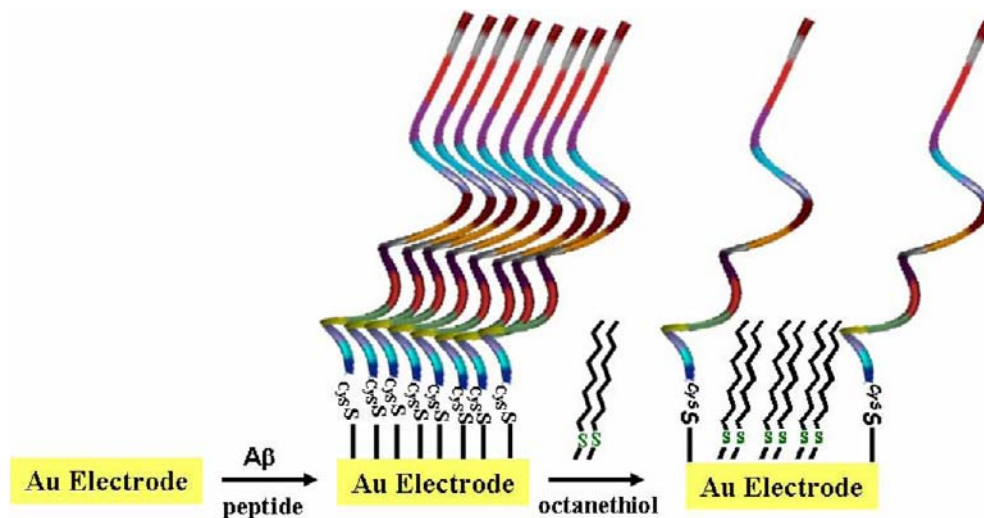


**Figure 1.** AFM images of  $A\beta_{Cys}$  SAM covered surfaces. 3D topology of (A) wall-like structure and (B) isolated clusters of  $A\beta_{Cys}$  SAM surfaces. (C)  $A\beta_{Cys}$  SAM covered surface ( $1 \times 1 \mu\text{m}^2$ ) with octanethiol diluent and (D) an enlarged view of a ( $0.5 \times 0.5 \mu\text{m}^2$ ) cross-section of (C).

### Scheme 1. Schematic Representation of $A\beta_{Cys}$ SAM Formation on Au Electrodes



## 3. RESULTS AND ANALYSIS

**3.1. Characterization of Surface.** **3.1.1. AFM.** Human  $A\beta(1-16)$  is appended with a cysteine residue ( $A\beta_{Cys}$ ) at the C-terminus. This thiol group of the cysteine residue has been used to form SAM on Au electrodes. AFM images of the surface generated after immersing clean Au wafers in a solution of  $A\beta_{Cys}$  show the presence of both large and small (Figure 1A, B, respectively) peptide aggregates. The aggregates are 5–9 nm high and 10–40 nm wide and extend from 0.1 to several  $\mu\text{m}$

(Figure 1A, B). Formation of these continuous wall-like features is consistent with similar aggregation of  $A\beta$  peptides reported on graphite and mica surfaces.<sup>43</sup> When these surfaces, bearing  $A\beta_{Cys}$  SAM, are immersed in a solution of long chain thiol (e.g., octanethiol), these wall-like features disappear, and a smooth homogeneous surface is formed, where small islands, 5–7 nm high, project out of the octanethiol SAM covered surface (Figure 1C, Scheme 1). The  $A\beta$  peptides are known to form  $\beta$ -sheets during aggregation.<sup>28</sup> The height of these islands is consistent

with formation of parallel  $\beta$  sheets (3.3 Å per residue, 17 residues  $\sim$ 5.5 nm).<sup>44</sup> The contact angle for these surfaces is measured to be 70.11°, which is less than bare Au (85.67°), indicating formation of SAM bearing significant hydrophilic character which may be expected for these water-soluble peptides. The nature of SAM does not change when heme is bound to these  $A\beta$  peptides (Figure S2, Supporting Information).

**3.1.2. Absorption Spectroscopy.** Binding heme to  $A\beta$  results in an intense Soret band, which can be monitored by absorption spectroscopy.<sup>18,19,38</sup> In homogeneous solution, a split Soret with  $\lambda_{\text{max}}$  of 391 nm and a shoulder at 363 nm is characteristic of the resting  $A\beta(1-16)$  bound heme complex.<sup>18</sup> Absorption data obtained on heme bound  $A\beta_{\text{Cys}}$  immobilized on transparent Au wafers show a similar split Soret (peak at 399 nm with shoulder at 370 nm, Figure 2, red). These differences may reflect differences

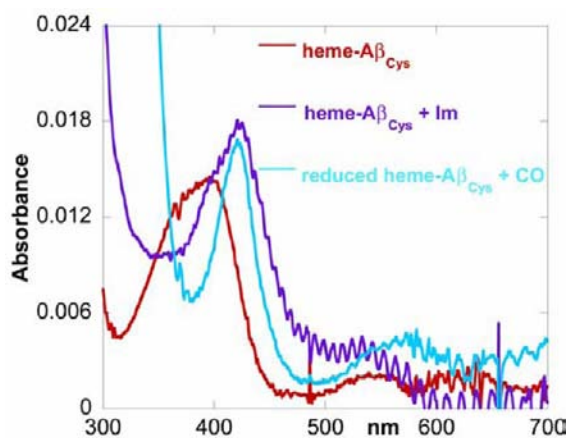


**Figure 2.** The absorption data of a single monolayer of heme bound  $A\beta_{\text{Cys}}$  (red), heme bound  $A\beta_{\text{Cys}}$  in 100 mM imidazole (purple), and reduced heme bound  $A\beta_{\text{Cys}}$  + CO (cyan) on Au electrodes.

in the heme environment between the heme- $A\beta$  complex in solution and the heme- $A\beta_{\text{Cys}}$  SAM (Figure S3, Supporting Information) and is better addressed with SERRS (Section 3.1.3).<sup>45</sup> The Soret band shifts to 426 nm on binding imidazole to heme- $A\beta_{\text{Cys}}$  SAM (Figure 2, purple, and S3A, Supporting Information), indicating a high- to low-spin transition upon binding a strong  $\sigma$  donor like imidazole.<sup>46</sup> Upon reduction and exposure to CO, a sharp Soret at 423 nm and reasonably resolved weaker bands at 545 and 577 nm are observed (Figure 2, cyan). These values are typical of ferrous CO adducts of histidine bound heme sites (the His<sup>13</sup> is known to bind heme).<sup>19,38,47,48</sup> Note that these data are collected on a monolayer on a transparent electrode surface. In spite of such dilution, the very high absorption coefficient of the heme cofactor ( $\epsilon = 10^5 \text{ mol}^{-1} \text{ cm}^{-1}$ ) results in discernible absorption features. On the contrary, Cu binding could not be monitored as d-d bands are very weak in intensity ( $\epsilon = 10-100 \text{ mol}^{-1} \text{ cm}^{-1}$ ).

**3.1.3. SERRS.** SERRS of the heme- $A\beta_{\text{Cys}}$  and resonance Raman data of heme- $A\beta$  in solution show significant similarities in the basic description of the site (Figure 3 A, B). The oxidation state, coordination number, and spin-state marker bands,  $\nu_4$ ,  $\nu_3$ , and  $\nu_2$  respectively, for both heme- $A\beta_{\text{Cys}}$  and heme- $A\beta$  in solution indicate the presence of a six-coordinate high-spin  $\text{Fe}^{3+}$  active sites (Figure 3A).<sup>49,50</sup> Note that SERRS of free heme physisorbed on octanethiol SAM (i.e., without  $A\beta_{\text{Cys}}$ ) and the SERRS of heme- $A\beta_{\text{Cys}}$  show the same differences as solution resonance Raman data of free heme and heme- $A\beta$  (Figure

S4A-C, Supporting Information).<sup>51</sup> The  $\nu_3$  vibration of heme- $A\beta$  complex in solution shows the presence of three species. The major species has a  $\nu_2$  and  $\nu_3$  at 1564 and 1494  $\text{cm}^{-1}$ , respectively, similar to that of a six-coordinate horseradish peroxidase (HRP) site.<sup>52</sup> There are two additional minor components in the  $\nu_3$  band: one at 1483  $\text{cm}^{-1}$  and the other at 1511  $\text{cm}^{-1}$  (Figure 3C). These indicate the presence of a six-coordinate high-spin Mb-type active site ( $\nu_3$  at 1483  $\text{cm}^{-1}$ ) and a six-coordinate low-spin active site ( $\nu_3$  at 1506  $\text{cm}^{-1}$ ) along with the major species with a HRP-type active site.<sup>50</sup> However the heme- $A\beta_{\text{Cys}}$  complex on the surface shows only two of the three components present in heme- $A\beta$  in solution (Figure 3D). These two components have  $\nu_3$  vibrations at 1483 and 1491  $\text{cm}^{-1}$  representing the Mb-type and the HPR-type six-coordinate high-spin species, respectively. The relative intensities of these components indicate that the population of the Mb type species with a  $\nu_3$  at 1483  $\text{cm}^{-1}$  (component II, Figure 3C, D) is more in heme- $A\beta_{\text{Cys}}$  relative to heme- $A\beta$  in solution. Although the comparison between the solution and SAM data is slightly complicated by the presence of scattering from sample tubes used to obtain the solution data (Figure 3 marked by \*), the low-energy region also shows an overall similarity between the two species (Figure 3B). The Fe-N (pyrrole) vibration of the heme- $A\beta$  complex in solution (351  $\text{cm}^{-1}$ ) is slightly higher in energy relative to the same vibration in heme- $A\beta_{\text{Cys}}$  (348  $\text{cm}^{-1}$ ). This may be due to the presence of a minority low-spin species in the heme- $A\beta$  complex in solution, which is generally characterized by a higher Fe-N (pyrrole) vibration. There is a vibration at  $\sim$ 420  $\text{cm}^{-1}$  in both the heme- $A\beta$  complex in solution and the heme- $A\beta_{\text{Cys}}$  SAM, which may be the Fe-OH<sub>2</sub> stretching frequency. The in-plane symmetric pyrrole deformation at 678  $\text{cm}^{-1}$  and the out-of-plane pyrrole deformations between 700 and 800  $\text{cm}^{-1}$  retain their position and relative intensities. This indicates a similar environment of the heme cofactor in the heme- $A\beta$  solution and heme- $A\beta_{\text{Cys}}$  SAM surfaces.

SERRS of heme- $A\beta_{\text{Cys}}$  and the imidazole bound heme- $A\beta_{\text{Cys}}$  show the  $\nu_4$ ,  $\nu_3$ , and the  $\nu_2$  bands at 1373, 1495, and 1569  $\text{cm}^{-1}$  and 1375, 1508, and 1595  $\text{cm}^{-1}$ , respectively (Figure 4). These values indicate that the major six-coordinate high-spin  $\text{Fe}^{3+}$  heme- $A\beta_{\text{Cys}}$  species is converted to a six-coordinate low-spin  $\text{Fe}^{3+}$  species on imidazole binding.<sup>48,49</sup> Free heme physisorbed on an octanethiol electrode also shows a similar spin change on imidazole addition (Figure S5A, Supporting Information), although the SERRS data of the imidazole bound free heme are significantly different from that of imidazole bound heme- $A\beta_{\text{Cys}}$  (Figure S5B, Supporting Information). The absorption data of heme physisorbed on octanethiol in the presence of 100 mM imidazole and heme- $A\beta_{\text{Cys}}$  SAM in the presence of 100 mM imidazole are also different (Figure S6, Supporting Information). Thus both the SERRS and absorption data indicate that exogenous imidazole is not competing with  $A\beta_{\text{Cys}}$  for binding heme, i.e. heme does not dissociate from  $A\beta_{\text{Cys}}$  on imidazole addition.

**3.2. Electrochemical Properties.** **3.2.1. CV.** Cu- $A\beta_{\text{Cys}}$  in air saturated pH 7 buffer shows a quasireversible CV at 0.1 V and a weak electrocatalytic O<sub>2</sub> reduction current (Figures 5 and 6 and Supporting Information).<sup>53</sup> On the contrary, heme- $A\beta_{\text{Cys}}$  shows a large O<sub>2</sub> reduction current at -0.49 V (Figure 5, red). Consequently no  $\text{Fe}^{3+/2+}$  CV could be observed under these conditions.<sup>54</sup> When both Cu and heme were loaded, the O<sub>2</sub> reduction by heme is shifted to -0.47 V (Figure 5, green). In the absence of O<sub>2</sub>, i.e., in degassed buffer, the Cu<sup>2+/+</sup> CV is clearly visible at 0.1 V, and the heme  $\text{Fe}^{3+/2+}$  CV is observed at -0.35 V

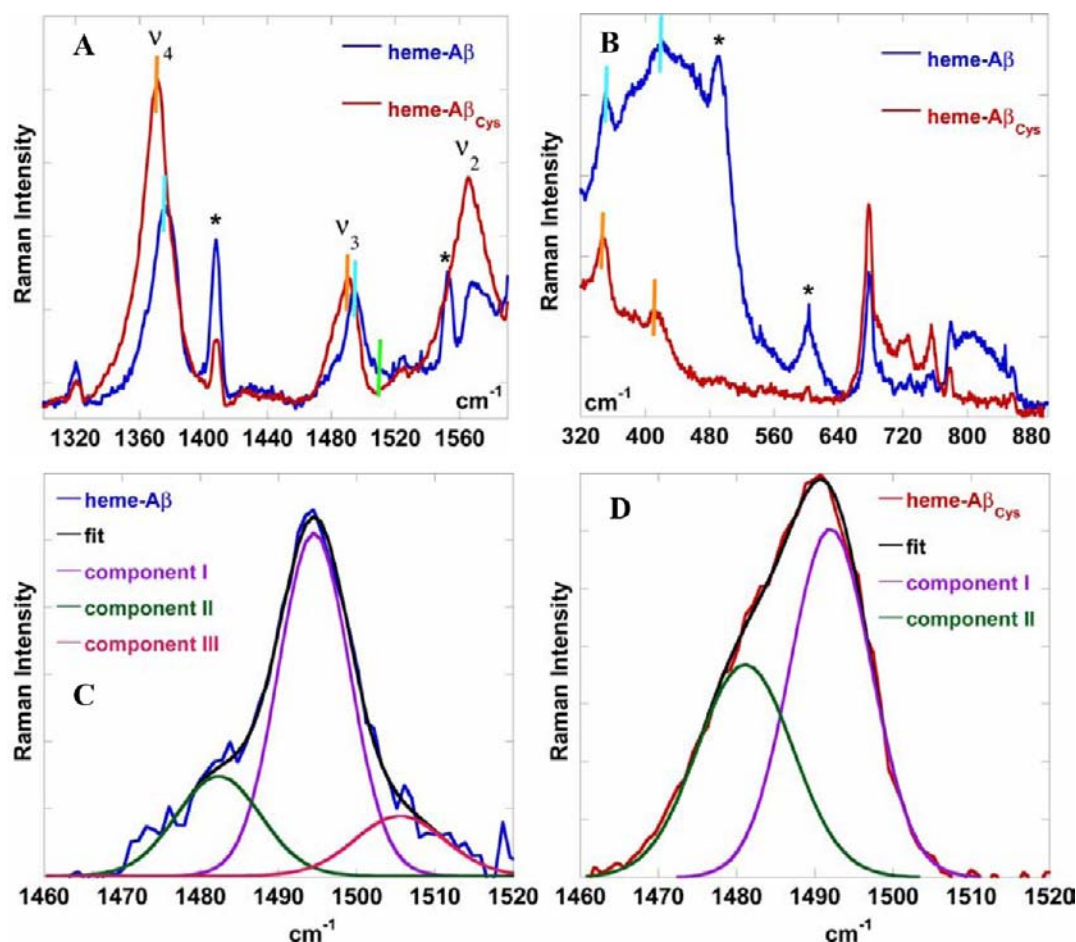


**Figure 3.** Solution rR of heme- $A\beta$  (blue) and SERRS of heme- $A\beta_{Cys}$  (red) in the (A) high-energy and (B) low energy regions. The peaks marked \* are either plasma lines or derived from scattering from sample tubes.  $\nu_3$  bands of (C) heme- $A\beta$  and (D) heme- $A\beta_{Cys}$  with fits showing different components.

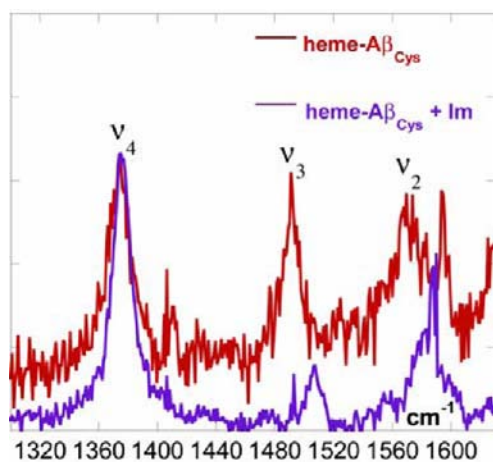


**Figure 4.** The SERRS data of a single monolayer of heme bound  $A\beta_{Cys}$  (red) and heme bound  $A\beta_{Cys}$  in 100 mM imidazole (purple) on Ag disk.

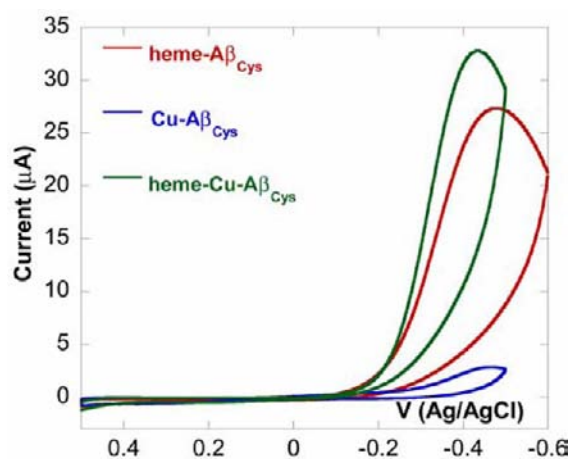


**Figure 5.** CV data of heme bound, copper bound, and both heme and copper bound  $A\beta_{Cys}$  in air saturated pH 7 buffer.

for the heme-Cu complex of  $A\beta_{Cys}$  SAM (Figure S9, Supporting Information). The integrated area under the cathodic wave is a direct and quantitative estimate of the amount of redox active species bound to an electrode.<sup>39,55–57</sup> The experimental integrated charges are the same for both  $Cu^+$  and heme  $Fe^{2+}$  oxidation, implying that the ratio of Cu:heme in these complexes is 1:1, similar to that observed in homogeneous solutions of

heme-Cu- $A\beta$  complexes.<sup>26</sup> The integrated charges under these peaks indicate that the number of Cu and heme sites present is  $\sim 0.5\text{--}1.0 \times 10^{12}$  per  $cm^2$ . Thus a normal  $0.5\text{ cm}^2$  electrode surface bears  $0.5 \times 10^{-11}$  moles, i.e., 5 pmol of the active site. Note that SAM of  $A\beta$  peptides on Au wafers completely abolishes the electrocatalytic  $O_2$  reduction exhibited by the bare Au electrodes (Figure S10, Supporting Information). Immersion

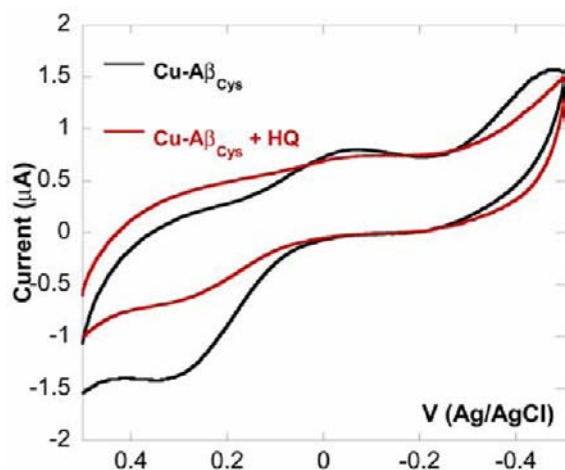


**Figure 6.** CV data of Cu- $A\beta_{Cys}$  surfaces in the absence (black) and the presence of 15 nM HQ (red) in pH 7 buffer.

of these surfaces in octanethiol results in a much better insulation of the electroactive Au surfaces from the conducting solution (Figure S10, Supporting Information).

**3.2.2.  $O_2$  Reduction. 3.2.2.1. Wild Type (WT).** The reaction of  $O_2$  with reduced Cu- $A\beta$  or heme- $A\beta$  complexes leads to the formation of  $H_2O_2$ .<sup>26</sup> This is because the Cu or the heme active site alone does not possess four electrons required to reduce  $O_2$  to  $H_2O$ . When immobilized on an electrode the additional electrons needed could be provided by the electrode at sufficiently reduced potentials. However at intermediate potentials, PROS are produced due to the incomplete reduction of  $O_2$  which can be detected *in situ* under steady-state conditions using RRDE. The amount of PROS released by Cu- $A\beta_{Cys}$  is  $31 \pm 1\%$  at  $-0.2$  V (i.e., 0 V vs NHE). This implies that 31% of the electrocatalytic  $O_2$  reduction current represents the reduction of  $O_2$  to  $H_2O_2$ . The remaining 69% PROS remains unobserved possibly because of the formation of  $H_2O$  instead of  $H_2O_2$  because of the ready availability of electrons from the electrodes. In contrast, PROS generated is  $17 \pm 2\%$  for heme- $A\beta_{Cys}$  and  $23 \pm 3\%$  for heme-Cu  $A\beta_{Cys}$  (Table 1) at  $-0.2$  V (i.e., 0 V vs NHE).

**Table 1.** PROS Produced by  $A\beta$  Complexes at pH 7

cofactor	Cu	heme	heme-Cu
WT	$31 \pm 1\%$	$17 \pm 2\%$	$23 \pm 3\%$
Tyr <sup>10</sup> Gly	$13 \pm 1\%$	$7 \pm 1\%$	$7 \pm 3\%$
Arg <sup>5</sup> Gly	$20 \pm 5\%$	$9 \pm 3\%$	$11 \pm 1\%$

**3.2.2.2. Mutants.** His<sup>13</sup> (involved in heme binding), Tyr<sup>10</sup>, and Arg<sup>5</sup> are the three residues absent in rodents (rodents do not get affected by AD) and may have significant implications in AD.<sup>26,38,58</sup> Reduced Cu- $A\beta$  is known to reduce  $O_2$  by two electrons to  $H_2O_2$  under homogeneous conditions.<sup>59–61</sup> While one electron required for the process is derived from  $Cu^+$ , which gets oxidized to  $Cu^{2+}$ , the other electron is donated by the Tyr<sup>10</sup> residue.<sup>26</sup> Subsequently the PROS produced by the Tyr<sup>10</sup>Gly mutant of Cu- $A\beta_{Cys}$  is 13%, i.e., close to half of the WT (Table 1). This implies that the PROS observed in Cu- $A\beta_{Cys}$  results from the two-electron reduction of  $O_2$  to  $H_2O_2$ , where one electron is derived from Cu and the other from Tyr<sup>10</sup>. In the absence of this residue, only one electron is donated by the metal cofactor to  $O_2$ . This reduces  $O_2$  to  $O_2^-$  which then disproportionates to produce half of an equivalent of  $H_2O_2$ . The PROS

produced by the Tyr<sup>10</sup>Gly mutants of heme- $A\beta_{Cys}$  and heme-Cu- $A\beta_{Cys}$  complexes are decreased to  $7 \pm 1\%$  and  $7 \pm 3\%$ , respectively (Table 1), further indicating the role of Tyr<sup>10</sup> in PROS formation.

Furthermore the Cu bound, the heme bound, and the heme and Cu bound Arg<sup>5</sup>Gly mutant of  $A\beta_{Cys}$  shows  $20 \pm 5\%$ ,  $9 \pm 3\%$ , and  $11 \pm 1\%$  PROS (Table 1), respectively. Thus, in all of these complexes, the amounts of PROS generation are significantly reduced when the Arg<sup>5</sup> residue is mutated to Gly. This may imply that the hydrogen-bonding Arg<sup>5</sup> residue may assist in  $H_2O_2$  production in these complexes.

**3.3. Inhibitors.** 8-hydroxyquinoline (HQ) has the basic scaffold of the drug cloiquinol (5-chloro-7-iodo-quinolin-8-ol). It is known to be a weak Cu chelator. It has been proposed that cloiquinol removes Cu bound to  $A\beta$  and relieves oxidative stress in brain cells.<sup>16</sup> When a Cu loaded  $A\beta_{Cys}$  SAM is immersed in a (15 nM) solution of HQ in pH 7 buffer, the Cu<sup>2+/+</sup> CV disappears (Figure 6). No new CV appears in the range of 0.5 to  $-0.5$  V. Heme- $A\beta_{Cys}$  SAM in the presence of HQ shows no significant effect on  $O_2$  reduction. The disappearance of the Cu<sup>2+/+</sup> CV indicates that HQ likely removes the Cu bound to  $A\beta_{Cys}$  due to its chelate effect.

MB is a potential drug aimed at ameliorating the negative effects of heme binding to  $A\beta$  peptides.<sup>37</sup> It is unknown how this potential therapeutic agent interacts with  $A\beta$  peptides or the heme- $A\beta$  complex. Incubation of the heme- $A\beta_{Cys}$  SAM with 15  $\mu$ M MB for a period of six hours or more significantly lowers the  $O_2$  reduction by the heme- $A\beta_{Cys}$  complex (Figure 7, blue).

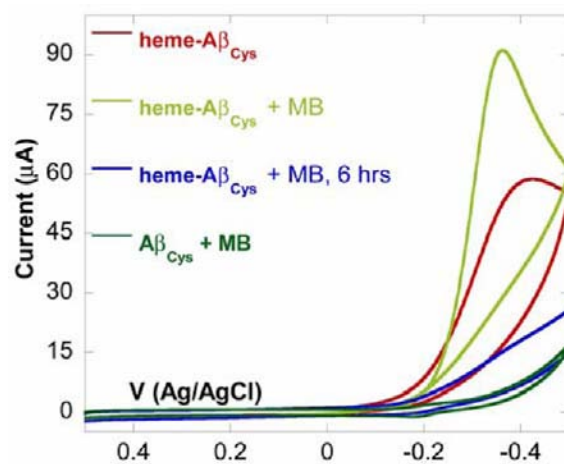


**Figure 7.** CV of heme- $A\beta_{Cys}$  (red), heme- $A\beta_{Cys}$  + MB after instantaneous addition (green), heme- $A\beta_{Cys}$  + MB after 6 h of incubation (blue), and  $A\beta_{Cys}$  + MB (dark green) in air saturated pH 7 buffer.

Instead of the strong  $O_2$  reduction current, a CV is observed at  $-170$  mV (Figure 7, blue). This CV is also observed when  $A\beta_{Cys}$  SAM surface or octanethiol SAM is independently incubated with MB for six hours or more (Figure 7, dark green) and represents the redox process of MB absorbed on these surfaces. Note that the CV of heme physiadsorbed on an alkanethiol SAM after six hours of incubation with MB shows a strong  $O_2$  reduction current (Figure S11, Supporting Information). The absorption data of these MB incubated surfaces show the presence of the heme- $A\beta$  bound to the electrode (Figure S12, Supporting Information), implying that the loss of  $O_2$  reduction is not because of the loss of heme from the SAM.<sup>62</sup> Furthermore,

the amount of PROS generated by the heme cofactor in the presence of MB adsorbed on the surface, corresponding to the residual  $O_2$  reduction current, is  $8 \pm 2\%$ , which is significantly lower than that observed for heme- $A\beta_{Cys}$  SAM (Table 1).

The inhibition of  $O_2$  reduction of heme- $A\beta_{Cys}$  by MB and reduction in the amount of PROS generated may be due to the direct interaction of MB with heme cofactor. This is confirmed by titrating heme- $A\beta$  with MB in a homogeneous solution (Figure 8). The absorption data show significant redistribution of

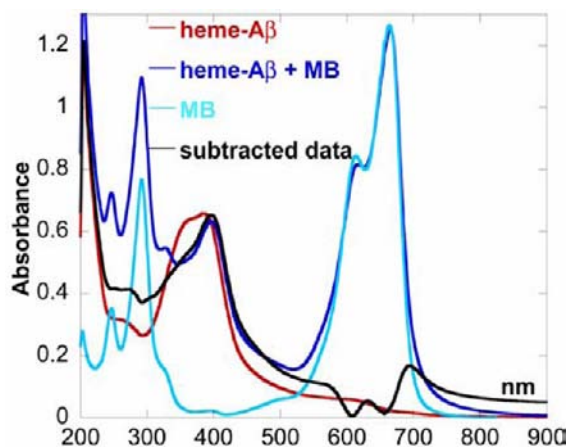


**Figure 8.** Absorption data of MB (light blue), heme- $A\beta$  (red), and their complex (dark blue). The black line indicates the difference between the absorption by the heme- $A\beta$ -MB complex and free MB.

intensity in the Soret region of heme- $A\beta$  upon addition of 1 equiv of MB (data in the Q-band region is obscured by charge-transfer bands of MB). This shift is clearer in the difference spectrum (Figure 8, black) which indicates that both the MB and the heme- $A\beta$  spectra are perturbed. This suggests the presence of a direct interaction of MB with heme- $A\beta$  complex. Heme and heme enzymes are known to bind MB in solution.<sup>63</sup> However, the absorption data alone are inconclusive, and vibrational data may offer more information (*vide infra*).

SERRS data of the MB incubated heme- $A\beta$  surfaces indicate formation of a new species. The  $\nu_4$  and  $\nu_2$  bands are at 1371 and 1567  $cm^{-1}$ , respectively, indicating that the heme is still bound to the peptide with the Fe in its +3 oxidation state (Figure 9A).

The  $\nu_3$  band shows only one component at 1489  $cm^{-1}$  for the MB incubated surface instead of two components observed for the heme- $A\beta_{Cys}$  SAM (Figure 9A). Thus the MB bound active site can be described as a six-coordinate high-spin species.<sup>50</sup> The shift of the  $\nu_4$ ,  $\nu_3$ , and  $\nu_2$  vibrations and the change in their relative intensities reflect significant perturbation of the active site. In the low-frequency region the out-of-plane  $\nu_7$  vibration at 679  $cm^{-1}$  of heme- $A\beta$  shifts to 675  $cm^{-1}$  (Figure 9B). There is a new band at 390  $cm^{-1}$  in the MB incubated surface (Figure 9B). This may reflect a Fe-N stretch originating from MB binding to heme- $A\beta$  active site (the coordination from the S atom of MB is unfavorable due to steric factors). Simultaneously, the  $\nu_8$ ,  $\nu_7$ , and the  $\nu_{15}$  vibrations between 670 and 800  $cm^{-1}$ , which represent the Fe-N stretch, the in-plane symmetric pyrrole deformation, and breathing modes, respectively, (which are sensitive to axial ligands) shift on MB incubation. Thus, both the absorption and the SERRS data indicate a direct interaction of MB with the heme- $A\beta_{Cys}$  surface.

#### 4. DISCUSSION

SAM of cysteine terminated  $A\beta$  peptide,  $A\beta_{Cys}$ , is formed on Au electrodes. These peptides form large or small aggregates of vertical  $\beta$ -sheets depending on the absence or presence of additional coadsorbant thiols (Figure 1 and Scheme 1). Cu and heme can bind these peptides in 1:1 stoichiometric ratio. The thermodynamic potentials of these sites match those obtained for their native  $A\beta$  peptide complexes in solution. Absorption and SERRS data of the heme- $A\beta$  and the heme- $A\beta_{Cys}$  complexes show minor differences between these heme active sites (Figure 3, and S3, S4, Supporting Information). In particular, the  $\nu_3$  vibration of heme- $A\beta_{Cys}$  complex shows presence of a dominant six-coordinate high-spin HRP-type active site and another minor six-coordinate high-spin Mb-type active site. The resonance Raman data of the heme- $A\beta$  complex in solution indicate the presence of a minor six-coordinate low-spin active site species in addition to the high-spin HRP- and MB-type active sites. While the peroxidase-type active site may be expected in heme- $A\beta$  (it is proposed to have some peroxidase activity),<sup>18</sup> the origin of the minor Mb type active site is not clear at this point. It likely indicates the presence of an alternate conformation where the Arg<sup>5</sup> residue is absent in the distal pocket.

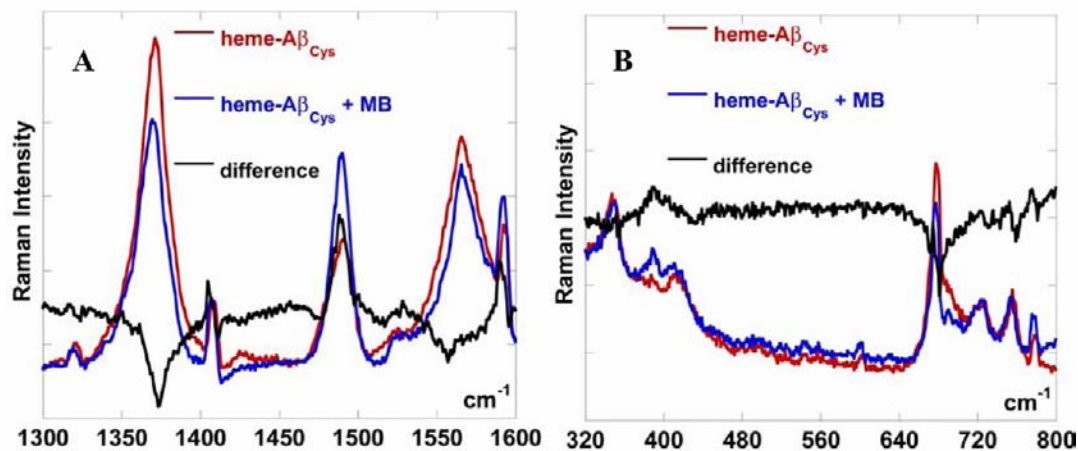


**Figure 9.** The SERRS data of a single monolayer of heme bound  $A\beta_{Cys}$  (red) and heme- $A\beta_{Cys}$  bound MB (blue) on Ag disk. The black line indicates the difference between the SERRS data of heme- $A\beta_{Cys}$ -MB complex and heme- $A\beta_{Cys}$ . (A) high-frequency and (B) low-frequency regions.

The Cu–A $\beta$ <sub>Cys</sub> active sites exhibit a quasireversible Cu<sup>2+/+</sup> CV at 0.1 V in the absence of O<sub>2</sub> at pH 7. Under aerobic conditions the Cu–A $\beta$ <sub>Cys</sub> shows very weak electrocatalytic O<sub>2</sub> reduction at pH 7 (Figure 5). Previous attempts of delineating the O<sub>2</sub> reduction activity of this metal center were complicated by the background O<sub>2</sub> reduction by the working electrodes and by the presence of free copper in solution due to relatively weak Cu binding to A $\beta$ .<sup>64–66</sup> In the present experimental setup both of these factors have been eliminated: the SAM formation shields the electrode from directly reducing O<sub>2</sub> (minimal background O<sub>2</sub> reduction, Figure S10, Supporting Information), and immobilization of A $\beta$  on the electrode ensures complete removal of unbound Cu ions during washing. Moreover, no decrease in the Cu signal in CV data after washing the electrodes several times (Figure S1, Supporting Information) and during repeated CV scans during the course of the experiment is observed, implying that Cu does not dissociate from the active site during redox cycling. This is in contrast to results obtained in solution and possibly reflects differences in Cu<sup>2+/+</sup> binding affinity between A $\beta$  in solution and A $\beta$  aggregates on the surface. Heme–A $\beta$ <sub>Cys</sub> shows greater O<sub>2</sub> reduction currents compared to Cu–A $\beta$ <sub>Cys</sub>, indicating that it is more kinetically competent in O<sub>2</sub> reduction (Figure 5). Further, the Cu site produces twice as much PROS as the heme site. Thus given the higher potential of Cu–A $\beta$ <sub>Cys</sub> (0.1 V vs Ag/AgCl, i.e., 0.3 V vs NHE) relative to heme–A $\beta$ <sub>Cys</sub> (–0.34 V vs Ag/AgCl, i.e., –0.13 V vs NHE), the Cu–A $\beta$ <sub>Cys</sub> site is more likely to be in the reduced Cu<sup>+</sup> state under physiological conditions, which is more toxic for PROS formation. Thus one may envisage that the Cu–A $\beta$ <sub>Cys</sub> is capable of more long-term oxidative stress than heme–A $\beta$ <sub>Cys</sub>.

In homogeneous solution both Cu–A $\beta$  and heme–A $\beta$  complexes produce 100% PROS, i.e., 1 equiv of O<sub>2</sub> is reduced to 1 equiv of H<sub>2</sub>O<sub>2</sub>. One of the two electrons required to reduce O<sub>2</sub> to H<sub>2</sub>O<sub>2</sub> is provided by the reduced heme or Cu site (where the Fe<sup>2+</sup> gets oxidized to Fe<sup>3+</sup> or Cu<sup>+</sup> gets oxidized to Cu<sup>2+</sup>), and the other electron is donated by the redox active Tyr<sup>10</sup> residue. Unlike the homogeneous conditions, direct electron transfer from the electrode, upon immobilization of these active sites on the electrode, generally favors complete reduction of O<sub>2</sub> to H<sub>2</sub>O which will produce no PROS. Thus the 17% PROS observed for heme–A $\beta$ <sub>Cys</sub> (Table 1) in RRDE (and not 100% as heme–A $\beta$  in solution) results from two competing reactions: (1) the hydrolysis of the Fe<sup>III</sup>–O<sub>2</sub><sup>–</sup> or Fe<sup>II</sup>–OOH adduct resulting in PROS formation and (2) the electron transfer from the electrode further reducing O<sub>2</sub> to H<sub>2</sub>O. The Tyr<sup>10</sup> mutant produces only 13 ± 1% and 7 ± 1% PROS (i.e., half of the WT) for Cu–A $\beta$ <sub>Cys</sub> and heme–A $\beta$ <sub>Cys</sub> SAM, respectively, indicating that it is indeed involved in donating one electron to O<sub>2</sub>, producing H<sub>2</sub>O<sub>2</sub> which is detected in the RRDE experiments.

The Arg<sup>5</sup> residue is not directly involved in binding either heme or Cu but has been invoked to be involved in second sphere interaction (possibly hydrogen bonding) with the ligands bound to the active site.<sup>67,68</sup> The results obtained here indicate that this interaction increases the production of PROS in these active sites. Hydrogen-bonding interaction with this Arg group (which remains protonated at physiological pH) increases the hydrolysis of metal bound O<sub>2</sub><sup>–</sup> or HOO<sup>–</sup> ligands (derived during incomplete reduction of O<sub>2</sub> by the reduced metal sites) producing PROS. The results (Table 1) indicate that the Arg<sup>5</sup> residue is poised to interact with both the heme and the Cu sites. The absence of the Arg<sup>5</sup> residue reduces PROS generation by the Cu site by 35% and by the heme site by 47%. In fact, in the case of heme–A $\beta$  complex, such hydrogen-bonding interaction of the

Arg<sup>5</sup> residue has been proposed to be present in the distal pocket, inducing the observed peroxidase activity.<sup>18</sup>

The Cu and heme bound A $\beta$ <sub>Cys</sub> SAM reproduce many of the spectroscopic and electrochemical properties exhibited by the Cu and heme bound complexes in solution. These surfaces provide a platform for directly probing the reactivity of these active sites and their interactions with potential drug molecules. Chelating molecules like clioquinol have Cu binding affinity higher than A $\beta$  peptides and thus remove Cu bound to A $\beta$  by chelation.<sup>16</sup> The Cu–A $\beta$ <sub>Cys</sub> SAM essentially reproduces this effect when a clioquinol analogue (HQ) is used. A clear loss of Cu<sup>2+/+</sup> CV on incubating these surfaces with >15 nM HQ indicates loss of Cu (Figure 6). MB, a potential drug for AD, inhibits O<sub>2</sub> reduction by heme–A $\beta$ . Solution absorption data of heme–A $\beta$  incubated MB complex (Figure 8) and absorption and SERRS data on the MB incubated heme–A $\beta$ <sub>Cys</sub> surface (Figure 9, S12, Supporting Information) indicate significant perturbation of the heme–A $\beta$  and heme–A $\beta$ <sub>Cys</sub> active sites, respectively. A new vibration is observed at 390 cm<sup>–1</sup> which may represent a Fe–N (N from MB) stretch implying a direct interaction of heme–A $\beta$ <sub>Cys</sub> with MB. Further, significant loss of O<sub>2</sub> reduction current on MB incubation of heme–A $\beta$ <sub>Cys</sub> implies that MB possibly acts as a competitive inhibitor of O<sub>2</sub>. The electrochemical data on the MB incubated surface also suggest that MB can act as an antioxidant as it lowers the PROS formation during the residual O<sub>2</sub> reducing activity by ~47%. Both the above effects may reduce the toxicity of heme–A $\beta$  significantly.

## 5. CONCLUSION

The approach described in this study provides a nonbiological platform for evaluating the effects of redox active cofactors in AD. The parallel monitoring of surface topology, electrochemical response, SERRS, and PROS production enables evaluation of aggregation properties, nature of active site formation, and its potential for inducing oxidative stress. Our results indicate that: (i) heme–A $\beta$  is catalytically more competent than Cu–A $\beta$  in reducing O<sub>2</sub>, (ii) Cu–A $\beta$  produces more PROS per mole of O<sub>2</sub> reduced than heme–A $\beta$  at physiological potentials, (iii) HQ (clioquinol analogue) chelates Cu ions and removes them from the A $\beta$  aggregates (no Cu<sup>2+/+</sup> CV is observed), and (iv) incubation of heme–A $\beta$  with MB results in significant inhibition of O<sub>2</sub> reduction. In principle this approach can be extended to understand other redox active metalloproteins, e.g., the prion proteins.

## ■ ASSOCIATED CONTENT

### 📄 Supporting Information

AFM, CV, solution resonance Raman, SERRS, and absorption data. This information is available free of charge via the Internet at <http://pubs.acs.org>.

## ■ AUTHOR INFORMATION

### Corresponding Author

icsgd@iacs.res.in; icad@iacs.res.in

### Author Contributions

†These authors contributed equally.

### Notes

The authors declare no competing financial interest.

## ■ ACKNOWLEDGMENTS

We thank the SERC Fast Track Scheme SR/FT/CS-34/2010 (SGD) and SR/S1/IC-35/2009 (AD), Department of Science

and Technology, Government of India for funding this research. We thank the CSIR, India, for Senior (D.P.) and Junior (K.S. and S.M.) Research Fellowships. Mr. Rabindranath Banik is thanked for collection of AFM data.

## REFERENCES

- (1) Maurer, I.; Zierz, S.; Moller, H. *Neurobiol. Aging* **2000**, *21*, 455.
- (2) Nelson, P. G. *Curr. Alzheimer Res.* **2005**, *2*, 497.
- (3) *Alzheimer's Disease International*. <http://www.alz.co.uk/>, accessed 1/10/2012.
- (4) *The Alzheimer's Association*. [http://www.alz.org/alzheimers\\_disease\\_alzheimer\\_statistics.asp](http://www.alz.org/alzheimers_disease_alzheimer_statistics.asp), accessed 1/10/2012.
- (5) Hardy, J.; Selkoe, D. J. *Science* **2002**, *297*, 353.
- (6) Selkoe, D. J. *Science* **2002**, *298*, 789.
- (7) Selkoe, D. J. *Nature* **1999**, *399*, A23.
- (8) Glenner, G. G.; Wong, C. W. *Biochem. Biophys. Res. Commun.* **1984**, *120*, 885.
- (9) Nunan, J.; Small, D. H. *FEBS Lett.* **2000**, *483*, 6–10.
- (10) Hou, L.; Shao, H.; Zhang, Y.; Li, H.; Menon, N. K.; Neuhaus, E. B.; Brewer, J. M.; Byeon, I. J.; Ray, D. J.; Vitek, M. P.; Iwashita, T.; Makula, R. A.; Przybyla, A. B.; Zagorski, M. G. *J. Am. Chem. Soc.* **2004**, *126*, 1992.
- (11) Klein, W. L.; Stine, W. B. *Nat. Rev. Mol. Cell. Biol.* **2007**, *8*, 101.
- (12) Masters, C. L.; Tanzi, R. E. *Proc. Natl. Acad. Sci. U.S.A.* **2003**, *100*, 11193.
- (13) Bush, A. I. *Trends Neurosci.* **2003**, *26*, 207.
- (14) Smith, D. J.; Cappai, R.; Barnham, K. J. *Biochim. Biophys. Acta* **2007**, *1768*, 1976.
- (15) Cherny, R. A.; Atwood, C. S.; Xilinas, M. E.; Gray, D. N.; Jones, W. D.; McLean, C. A.; Barnham, K. J.; Volitakis, I.; Fraser, F. W.; Kim, Y.-S.; Huang, X.; Goldstein, L. E.; Moir, R. D.; Lim, J. T.; Beyreuther, K.; Zheng, H.; Tanzi, R. E.; Masters, C. L.; Bush, A. I. *Neuron* **2001**, *30*, 665.
- (16) Cherny, R. A.; Legg, J. T.; McLean, C. A.; Fairlie, D. P.; Huang, X.; Atwood, C. S.; Beyreuther, K.; Tanzi, R. E.; Masters, C. L.; Bush, A. I. *J. Biol. Chem.* **1999**, *274*, 23223.
- (17) Atamna, H.; Frey, W. H., II *Proc. Natl. Acad. Sci. U.S.A.* **2004**, *101*, 11153.
- (18) Pramanik, D.; Dey, S. G. *J. Am. Chem. Soc.* **2011**, *1*, 81.
- (19) Atamna, H.; Boyle, K. *Proc. Natl. Acad. Sci. U.S.A.* **2006**, *103*, 3381.
- (20) Guilloureau, L.; Combalbert, S.; Sournia-Saquet, A.; Mazarguil, H.; Faller, P. *ChemBioChem* **2007**, *8*, 1317.
- (21) Curtain, C. C.; Ali, F.; Volitakis, I.; Cherny, R. A.; Norton, R. S.; Beyreuther, K.; Barrow, C. J.; Masters, C. L.; Bush, A. I.; Barnham, K. J. *J. Biol. Chem.* **2001**, *276*, 20466.
- (22) Palmer, A. M.; Burns, M. A. *Brain Res.* **1994**, *645*, 338.
- (23) Sayre, L. M.; Zelasko, D. A.; Harris, P. L. R.; Perry, G.; Salomon, R. G.; Smith, M. A. *J. Neurochem.* **1997**, *68*, 2092.
- (24) Mecocci, P.; MacGarvey, U.; Beal, M. F. *Ann. Neurol.* **1994**, *36*, 747.
- (25) Smith, D. P.; Smith, D. G.; Curtain, C. C.; Boas, J. F.; Pilbrow, J. R.; Ciccotosto, G. D.; Lau, T.-L.; Tew, D. J.; Perez, K.; Wade, J. D.; Bush, A. I.; Drew, S. C.; Separovic, F.; Masters, C. L.; Cappai, R.; Barnham, K. J. *J. Biol. Chem.* **2006**, *281*, 15145.
- (26) Pramanik, D.; Ghosh, C.; Dey, S. G. *J. Am. Chem. Soc.* **2011**, *133*, 15545.
- (27) Bao, Q.; Luo, Y.; Li, W.; Sun, X.; Zhu, C.; Li, P.; Huang, Z.; Tan, X. *J. Biol. Inorg. Chem.* **2011**, *16*, 809.
- (28) Rauk, A. *Chem. Soc. Rev.* **2009**, *38*, 2698.
- (29) Fassbender, K.; Simons, S.; Bergmann, C.; Stroick, M.; Lutjohann, D.; Kellerer, P.; Runz, H.; Kuhl, S.; Bertsch, T.; vonBergmann, K.; Hennerici, M.; Beyreuther, k.; Hartmann, T. *Proc. Natl. Acad. Sci. U.S.A.* **2001**, *98*, 5856.
- (30) Wolozin, B.; Wang, W. S.; Li, N.-C.; Lee, A.; Lee, T. A.; Kazis, L. E. *BMC Med.* **2007**, *5*, 20.
- (31) Vlad, S. C.; Miller, D. R.; Kowall, N. W.; Felson, D. T. *Neurology* **2008**, *70*, 1672.
- (32) McKee, A. C.; Carreras, I.; Hossain, L.; Ryu, H.; Klein, W. L.; Oddo, S.; LaFerla, F. M.; Jenkins, B. G.; Kowall, N. W.; Dedeoglu, A. *Brain Res.* **2008**, *1207*, 225.
- (33) Tanzi, R. E.; Bush, A. I. *Neurotherapeutics* **2008**, *5* (3), 421.
- (34) Butterfield, D. A. *Free Radical Res.* **2002**, *36*, 1307.
- (35) Beal, M. F. *Neurobiol. Aging* **2005**, *26*, 585.
- (36) Hirai, K.; Aliev, G.; Nunomura, A. *J. Neurosci.* **2001**, *21*, 3017.
- (37) Atamna, H.; Kumar, R. *J. Alzheimer's Dis.* **2010**, *20*, 439.
- (38) Atamna, H.; Frey, W. H., II; Ko, N. *Arch. Biochem. Biophys.* **2009**, *487*, 59.
- (39) Wei, J.; Liu, H.; Dick, A. R.; Yamamoto, H.; He, Y.; Waldeck, D. H. *J. Am. Chem. Soc.* **2002**, *124*, 9591.
- (40) Zhang, Y.; Wilson, G. S., J. *Electroanal. Chem.* **1993**, *345*, 253.
- (41) Hildebrandt, P.; Macor, K. A.; Czernuszewicz, R. S. *J. Raman Spectrosc.* **1988**, *19*, 65.
- (42) Bulovas, A.; Talaikytė, Z.; Niaura, G.; Kažemėkaitė, M.; Marcinkevičienė, L.; Bachmatova, I.; Meškys, R.; Razumas, V. *Chemija* **2007**, *18*, 9.
- (43) Kowalewski, T.; Holtzman, D. M. *Proc. Natl. Acad. Sci. U.S.A.* **1999**, *96*, 3688.
- (44) FTIR data will also confirm SAM formation.
- (45) Note that heme physioabsorbed on thiol SAM (i.e., no  $A\beta_{Cys}$ ) exhibits a different absorption spectrum than heme- $A\beta_{Cys}$  (Figure S2, Supporting Information).
- (46) Note that heme physioabsorbed on thiol SAM (i.e., no  $A\beta_{Cys}$ ) in 100 mM imidazole exhibits a different absorption spectrum than heme- $A\beta_{Cys}$  (Figure S3A, Supporting Information).
- (47) Smulevich, G.; Paoli, M.; Sanctis, G. D.; Mantini, A. R.; Ascoli, F.; Coletta, M. *Biochemistry* **1997**, *36*, 640.
- (48) Bowen, W. J. *J. Biol. Chem.* **1949**, *179*, 235.
- (49) Hu, S.; Smith, K. M.; Spiro, T. G. *J. Am. Chem. Soc.* **1996**, *118*, 12638.
- (50) Das, T. K.; Couture, M.; Lee, H. C.; Peisach, J.; Rousseau, D. L.; Wittenberg, B. A.; Wittenberg, J. B.; Guertin, M. *Biochemistry* **1999**, *38*, 15360.
- (51) Apart from the intensity differences in the  $\nu_4$ ,  $\nu_3$ , and  $\nu_2$  bands, the  $\nu_8$  band, which is assigned as the Fe-N(pyrrole) vibration, is  $11\text{ cm}^{-1}$  weaker than that of free heme. The value of this  $\nu_8$  vibration is consistent with coordination of a strong  $\sigma$  donor like histidine.<sup>48</sup>
- (52) Rakhit, G.; Spiro, T. G. *Biochemistry* **1974**, *13*, 5137.
- (53) No CV of Cu is observed in the absence of  $A\beta_{Cys}$  SAM (Figure S7, Supporting Information), as the Cu ion does not get absorbed on thiol surfaces.
- (54) Note that the CV of heme physioabsorbed on octanethiol SAM (i.e., no  $A\beta_{Cys}$ ) shows  $O_2$  reduction at much different potentials (Figure S8, Supporting Information)
- (55) Kadish, K. M.; Frémond, L.; Ou, Z.; Shao, J.; Shi, C.; Anson, F. C.; Burdet, F.; Gros, C. P.; Barbe, J.-M.; Guillard, R. *J. Am. Chem. Soc.* **2005**, *127*, 5625.
- (56) Collman, J. P.; Devaraj, N. K.; Eberspacher, T. P. A.; Christopher E. D. Chidsey, C. E. D. *Langmuir* **2006**, *22*, 2457.
- (57) Ferrero, V. E. V.; Andolfi, L.; Di Nardo, G.; Sadeghi, S. J.; Fantuzzi, A.; Cannistraro, S.; Gilardi, G. *Anal. Chem.* **2008**, *80*, 8438.
- (58) Atamna, H. *J. Bioenerg. Biomembr.* **2009**, *41*, 457.
- (59) Dikalov, S. I.; Vitek, M. P.; Mason, R. P. *Free Radical Biol. Med.* **2004**, *36*, 340.
- (60) Huang, X.; Moir, R. D.; Tanzi, R.; Bush, A. I.; Rogers, J. T. *Ann. N.Y. Acad. Sci.* **2004**, *1012*, 153.
- (61) Feaga, H. A.; Maduka, R. C.; Foster, M. N.; Szalai, V. A. *Inorg. Chem.* **2011**, *50*, 1614.
- (62) Note that observation of SERRS and absorption data are only possible if the chromophore is attached to the surface due to the surface enhancement phenomenon. Dissociation of  $10^{-12}$  moles of heme or Cu from the surface will result in a  $10^{-15}$  M solution (minimum volume required for absorption experiments using the existing setup is 1 mL), which is too dilute to produce any signal.
- (63) Atamna, H.; Krugliak, M.; Shalmiev, G.; Deharo, E.; Pescarmona, G.; Ginsburg, H. *Biochem. Pharmacol.* **1996**, *51*, 693.
- (64) Töögü, V.; Tiiman, A.; Palumaa, P. *Metallomics* **2011**, *3*, 250.

- (65) Rózga, M.; Bal, W. *Chem. Res. Toxicol.* **2010**, *2*, 298.
- (66) Faller, P.; Hureau, C. *Dalton Trans.* **2009**, *7*, 1080.
- (67) Eury, H.; Bijani, C.; Faller, P.; Hureau, C. *Angew. Chem., Int. Ed.* **2011**, *50* (4), 901.
- (68) Kowalik-Jankowska, T.; Ruta-Dolejsz, M.; Wisniewska, K.; Lankiewicz, L. *J. Inorg. Biochem.* **2001**, *86*, 535.